Wind Energy

WILEY

RESEARCH ARTICLE OPEN ACCESS

Climatic Impacts of Large-Scale Wind Farms in Arid and Semi-Arid Region in China: A Case Study of the Huitengxile Wind Farm in Inner Mongolia

Xiashu Su[1,2] | Entao Yu[2,3] | Dongwei Liu[1]

[1]School of Ecology and Environment, Inner Mongolia University, Hohhot, China | [2]Nansen-Zhu International Research Centre, Institute of Atmospheric Physics, Chinese Academy of Sciences, Beijing, China | [3]Collaborative Innovation Center on Forecast and Evaluation of Meteorological Disasters (CIC-FEMD), Nanjing University of Information Science & Technology, Nanjing, China

Correspondence: Entao Yu (yuet@mail.iap.ac.cn)

Received: 4 November 2025 | **Revised:** 20 June 2026 | **Accepted:** 2 July 2026

Keywords: arid and semi-arid regions | climatic effects | the WRF model | wind farm

ABSTRACT

With the rapid expansion of China's wind power industry, the local climatic impacts of large-scale wind farms, particularly in arid and semi-arid regions, have attracted increasing attention. This study investigates the effects of the Huitengxile wind farm in Inner Mongolia, which hosts over 1,200 wind turbines, using high-resolution numerical simulations conducted with the Weather Research and Forecasting (WRF) model. The analysis quantitatively evaluates the effects of the wind farm's influence on surface temperature, surface relative humidity, turbulent kinetic energy (TKE), and wind speed at turbine height by comparing control and sensitivity simulations. The results indicate that the Huitengxile wind farm induces a decrease in surface temperature but an increase in surface relative humidity. At hub height, TKE increases, while wind speed decreases within the wind farm area. These climatic responses exhibit seasonal and diurnal variability. In winter, the surface temperature decreases by approximately 0.5°C, wind speed reduces by 4.4 m/s, and TKE increases by 1.2 m^2/s^2. In contrast, summer responses are less pronounced, with surface temperature decreasing by 0.2°C, relative humidity increasing by 0.6%, wind speed reducing by 2.0 m/s, and TKE increasing by 0.7 m^2/s^2. Diurnal variations reveal stronger cooling, wetting, and wind speed reduction during nocturnal hours, whereas TKE enhancement is more significant during diurnal hours. Spatial analysis reveals that the wind farm's impacts are primarily confined to areas with high turbine density. These findings reveal the complex local climatic effects of large-scale wind farms, providing critical scientific insights for optimizing wind farm planning.

1 | Introduction

With the rapid development of the global economy, energy demand continues to rise [1]. The extensive use of traditional fossil fuels such as coal, oil, and natural gas has triggered a series of severe environmental issues, including global climate change caused by greenhouse gas emissions and air pollution [2–4]. To address these challenges, nations worldwide are actively promoting the development and utilization of renewable energy. Among these, wind energy has attracted significant attention because of its abundant resources, widespread availability, and clean, pollution-free nature [5–8]. Amid the rapid expansion of wind energy development and utilization, global wind farm construction has rapidly increased. While this trend offers new opportunities for sustainable energy production, it has also raised significant concerns about the localized climatic impacts of wind farms [9].

Early studies primarily relied on field observations to analyze the localized climatic impacts of wind farms. For instance,

TABLE 1 | Physical parameters used in WRF.

WRF physics	Parameterization scheme
Cumulus convective scheme	Off
Microphysics scheme	WRF Double-moment 6-class (WDM6) [32]
Radiation scheme	RRTMG [33]
Planetary boundary layer scheme	Mellor–Yamada Nakanishi and Niino Level 2.5 (MYNN2) ([34, 35]; [36])
Surface layer scheme	MYNN [37]
Land surface model scheme	Noah

Smith et al. [10] investigated near-surface flows at wind farms using in situ measurements from local meteorological towers; they examined diurnal and nocturnal variations in temperature, wind speed, and turbulent kinetic energy (TKE) caused by wind farm operations. Zhang et al. [11] analyzed meteorological station data from the Dabie Mountains region, indicating that wind farm operations exerted a certain degree of influence on local wind speeds and temperatures. Specifically, wind speeds showed a slight decrease while temperatures exhibited a noticeable increase, although no significant impact on precipitation was observed. In recent years, with continuous advancements in science and technology, methods such as satellite remote sensing and numerical simulation have been widely applied to studying the climatic effects of wind farms [12–17]. Among them, the Weather Research and Forecasting (WRF) model represents one of the most commonly used numerical models. Many studies indicate that wind farms can induce significant temperature change within and around the wind farm areas [18–21]. Sun et al. [22] utilized wind farm data and cumulative wind power capacity data from China, using the WRF model to simulate the regional environmental impacts of wind farms. Results showed that operational wind farms caused surface air temperatures at 2 m height to fluctuate within a range of ±0.5 K. Xia et al. [23] used the WRF model and found that wind farms induce warming within the wind farm areas and cooling in downwind areas during nocturnal periods. Baidya Roy [24] simulated a large wind farm in California, revealing significant impacts on near-surface air temperature, humidity, and surface sensible and latent heat fluxes, resulting in nocturnal warming and diurnal cooling of surface temperatures. Research has also shown that wind farms can significantly reduce wind speeds at turbine heights both within the wind farm and in downwind areas [25, 26]. Lundquist et al. [27] simulated adjacent wind farms in Texas using the WRF model, revealing wind speed deficiency of 0.5 m/s at 50 km downstream under stable atmospheric conditions. Fitch et al. [28] modeled the atmospheric impacts of a 10 × 10 km wind farm, demonstrating that operational wind farms significantly reduce wind speeds within a 60-km downwind radius during nocturnal hours. Moreover, research has demonstrated that wind farms significantly affect precipitation and sea level pressure [18, 29, 30]. Although numerous studies on wind farm climate impacts exist, most rely on observational data or low-resolution numerical simulations, with few high-resolution simulations at 1 km scale. Furthermore, previous studies primarily focused on small- to medium-scale wind farms, typically comprising a few hundred turbines or fewer, with limited research addressing large-scale wind farms containing thousands of turbines. Therefore, high-resolution simulations of the localized climatic effects of large-scale wind farms are urgently needed.

This study focuses on the Huitengxile wind farm in Inner Mongolia, which hosts more than 1200 wind turbines as a case study site. Employing the WRF model, we simulated the impacts of wind farm operations over the period from 2018 to 2020. And we examined the impact of the wind farm on surface air temperature, surface relative humidity, TKE, and wind speed at turbine height across different time scales. This study provides a scientific basis for the rational planning and optimized operation of wind farms. It also offers essential theoretical support and data references for assessing the environmental impacts of wind power development, formulating corresponding ecological protection measures, and promoting the sustainable development of renewable energy.

2 | Material and Methods

2.1 | Study Area

The Huitengxile wind farm is located at the junction of Chahar Right Middle Banner and Zhuozi County in Ulanqab City, Inner Mongolia Autonomous Region, China. It has an average elevation of 2100 m, an annual average temperature of approximately −1.3°C, and annual precipitation of about 385 mm [31]. The surrounding Huitengxile grassland is endowed with abundant wind energy resources and hosts approximately 1200 wind turbines. Characterized by high stability, excellent continuity, and superior wind resource quality, it serves as an ideal location for studying the impact of wind farms on local climate.

2.2 | The WRF Model

This study employed the WRF model version 4.6.1, and the primary physical parameterization schemes suitable for the study area were determined with reference to previous related simulation studies, as summarized in Table 1. The planetary

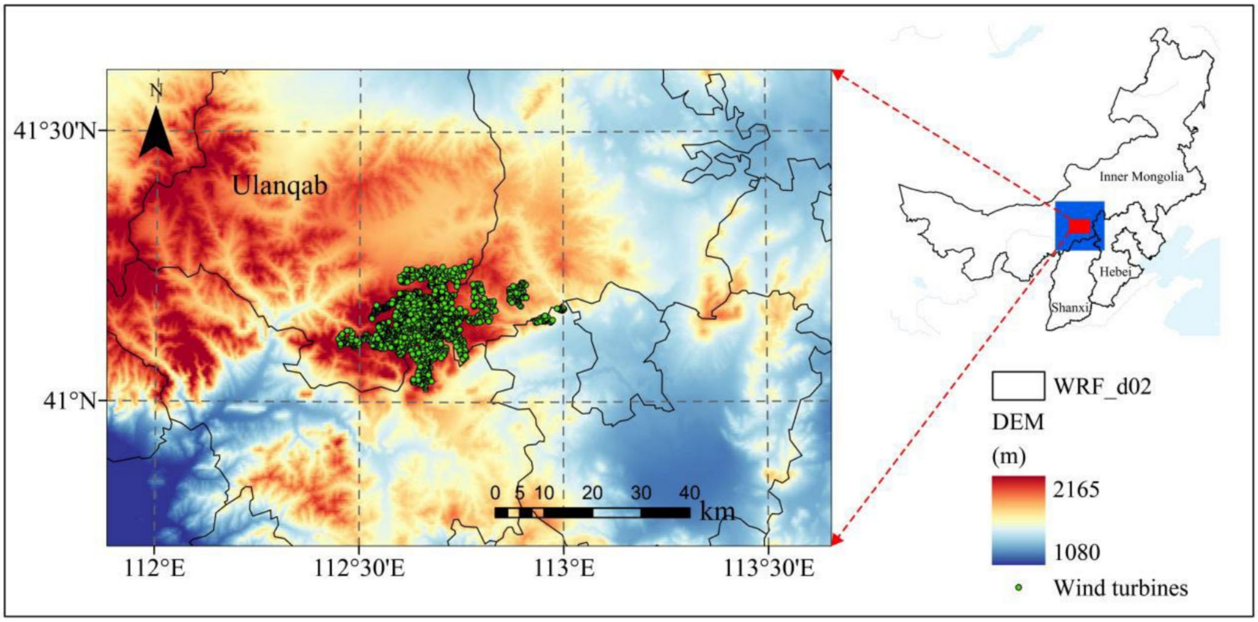

FIGURE 1 | Map of the WRF d02 simulation domain. Shading represents terrain elevation (units: meters), and wind turbines are indicated by green solid circles. The blue shading in the upper-right corner of the map denotes the WRF model d01 simulation domain.

boundary layer scheme adopts the Mellor–Yamada Nakanishi and Niino Level 2.5 scheme, which effectively simulates turbulence characteristics in stable and neutral boundary layers and has good applicability for simulating interactions between wind farms and the atmospheric boundary layer. The surface layer scheme employs the corresponding MYNN scheme to ensure consistency between the boundary layer and surface layer parameterizations. The microphysics scheme used is the WRF Double-moment 6-class scheme, which adequately simulates the cloud microphysical processes and precipitation characteristics of the study region. The radiation scheme used is the RRTMG scheme, which offers high computational accuracy and has been widely applied in regional climate simulations. Noah scheme is applied as the land surface scheme, which accurately describes the heat and moisture exchange processes over surfaces. The WRF model domain configuration is illustrated in Figure 1, centered at 41.2° N, 112.8° E. A two-way nested grid configuration was implemented, consisting of an outer domain with a 5-km horizontal resolution (70 grid points in both the east–west and north–south directions) that encompassed portions of Hohhot City, Ulanqab City, and surrounding areas, and an inner domain with a 1-km horizontal resolution (151 grid points in the east–west direction and 101 grid points in the north–south direction) focused on the construction area of the Huitengxile wind farm. The 5 km outer domain resolution effectively captures regional-scale atmospheric circulation features, while the 1 km inner domain resolution is sufficient to resolve the local climate responses within and around the wind farm, accurately characterizing the spatial distribution of wind turbines and their disturbance effects on local airflow, while maintaining computational efficiency. The simulation period spans from 2018 to 2020, with December 2017 serving as the model spin-up period. The simulation utilized the Lambert projection with the model top at 50 hPa. Model outputs were generated every 3 h and archived in NetCDF format.

The initial and boundary conditions for the WRF model are derived from the fifth-generation European Centre for Medium-Range Weather Forecasts (ECMWF) reanalysis dataset (ERA5), which integrates global observational and model data to produce a comprehensive, high-resolution record of atmospheric land surface and oceanic conditions [38, 39]. This dataset is widely adopted as the lateral boundary conditions in regional climate simulation over China [40]. In this study, ERA5 data with a horizontal resolution of 0.25° and a temporal resolution of 3 h were employed, and the wind farm parameterization scheme developed by Fitch et al. [41] was adopted, which fully considers the turbulent kinetic energy and momentum sink mechanisms and has been widely adopted.

2.3 | Experimental Design

In this study, the high-resolution sensitivity simulations were conducted to evaluate the impact of the wind farm on the local climate across four seasons from 2018 to 2020: winter (December–February), spring (March–May), summer (June–August), and autumn (September–November). Each day was further partitioned into diurnal (06:00–18:00 Beijing Time) and nocturnal (18:00–06:00 Beijing Time) periods [42] to examine the distinct diurnal and nocturnal responses to wind farm operations. The simulations include two experiments: a control run without the wind farm (Con) and a sensitivity run with the wind farm (WindFarm). The impact of the wind farm on local climate is represented by the difference between the two experiments, calculated as follows:

$$\Delta V = V_{WF} - V_{Con} \quad (1)$$

where ΔV denotes the impact of the wind farm on local climate, V_{WF} represents the simulated variable in the experiment of WindFarm, while V_{Con} represents the simulated variable in the Con experiment.

3 | Results

3.1 | Impact of Wind Farms on Local Surface Air Temperature

The process by which wind turbines convert kinetic wind energy into electrical energy alters the exchange and transport of atmospheric energy, momentum, and mass, thereby influencing near-surface atmospheric temperature. Figure 2 shows the spatial distribution of differences in surface temperature during different seasons. Within regions of high turbine density, surface temperatures show cooling, while surrounding regions exhibit relatively minor changes. The magnitude of the regional mean temperature decrease in winter, spring, summer, and autumn is approximately 0.23°C, 0.15°C, 0.07°C, and 0.10°C, respectively, while the corresponding natural variability for these four seasons is 1.31°C, 1.08°C, 0.86°C, and 1.11°C, respectively. These changes do not exceed the natural variability. The cooling effect is most pronounced in winter (Figure 2a), with a temperature reduction of approximately 0.5°C within the wind farm. In contrast, warming of about 0.3°C occurs in the northern and southeastern regions. During spring (Figure 2b) and autumn (Figure 2d) seasons, surface temperatures decrease by approximately 0.4°C within the wind farm and its northeastern areas, with negligible temperature differences in surrounding regions. In summer (Figure 2c), the surface temperature change is the weakest, with a mean cooling of approximately 0.2°C within the wind farm. Adjacent areas show slight warming in the northeast and minor cooling in the west, although these changes are of small magnitude.

Figure 3 shows the spatial distribution of mean surface temperature differences within the wind farm for diurnal and nocturnal periods. During diurnal periods (Figure 3a), the interior of the wind farm exhibits a modest cooling effect, with temperatures decreasing by approximately 0.16°C. Meanwhile, a warming effect is observed in the northern region of the wind farm. Overall, the influence of the wind farm on surface temperatures during diurnal periods is relatively minor. In contrast, during nocturnal periods (Figure 3b), the cooling effect is approximately three times greater than during diurnal periods. In areas with high wind turbine density, the maximum cooling reaches 0.44°C and exhibits distinct spatial clustering. This nocturnal cooling effect is primarily concentrated within the wind farm's interior, with a slight cooling effect in the northeastern region that gradually weakens with increasing distance from the turbine clusters.

Figure 4a,b illustrates the spatial distribution of mean surface temperature differences within the wind farm during diurnal and nocturnal periods in winter. During diurnal periods (Figure 4a), a cooling effect is observed in areas with concentrated wind turbine distribution, while warming occurs in the northern part of the wind farm. The nocturnal cooling effect is approximately three times greater than that during the diurnal

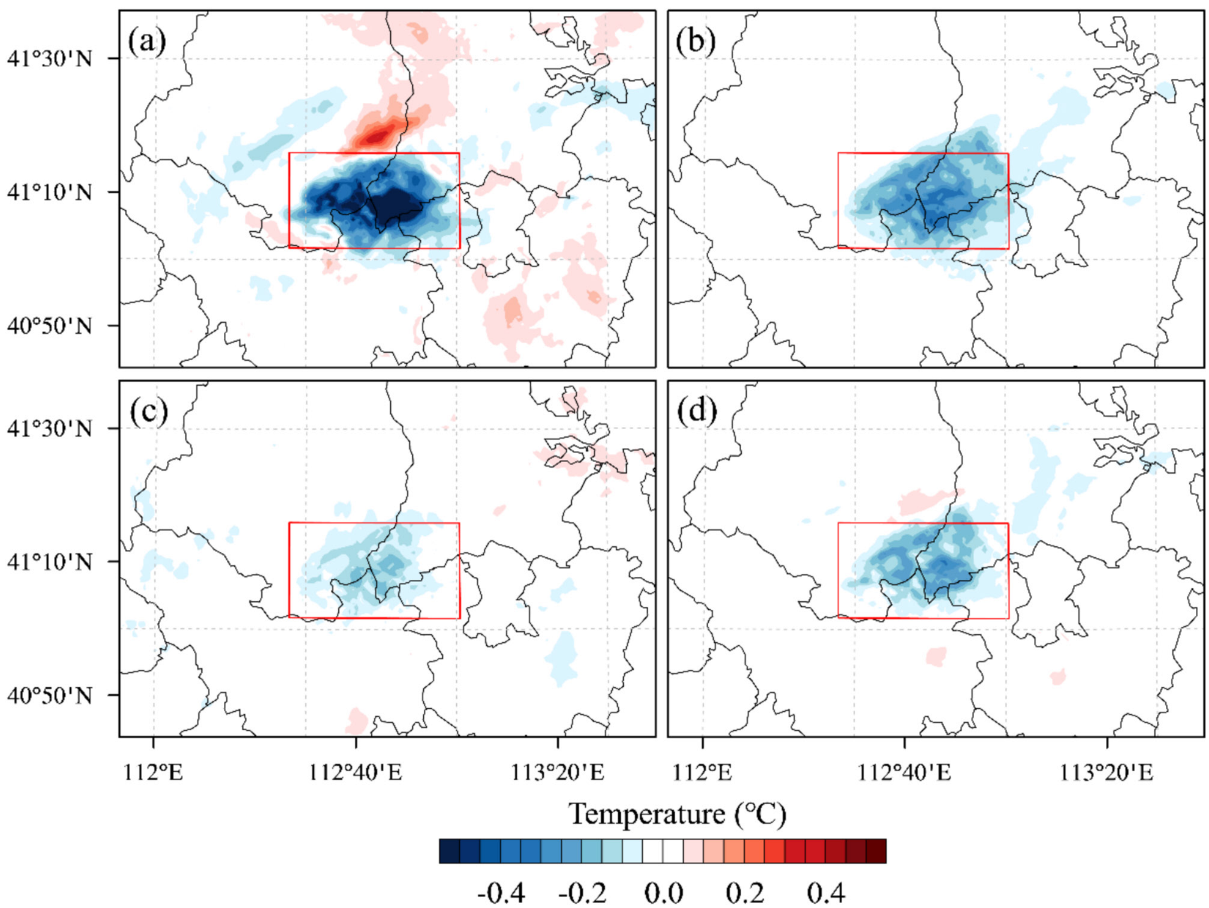

FIGURE 2 | Spatial distribution of mean surface air temperature differences within the wind farm for (a) winter, (b) spring, (c) summer, and (d) autumn. Red boxes indicate turbine locations. Units:°C.

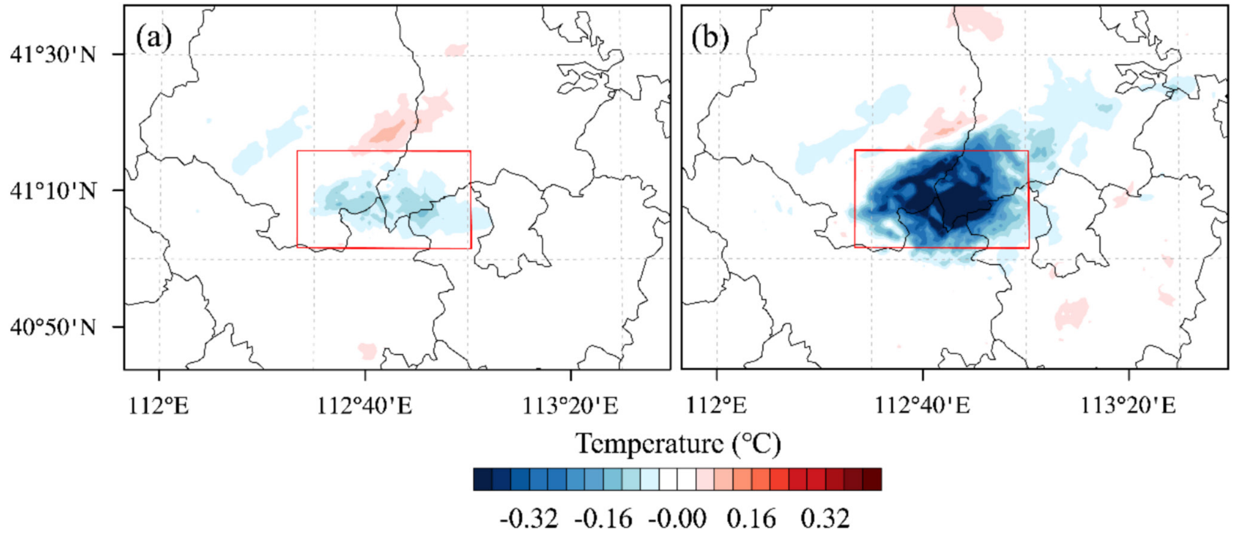

FIGURE 3 | Spatial distribution of mean surface air temperature differences for (a) diurnal and (b) nocturnal periods. Red boxes indicate turbine locations. Units:°C.

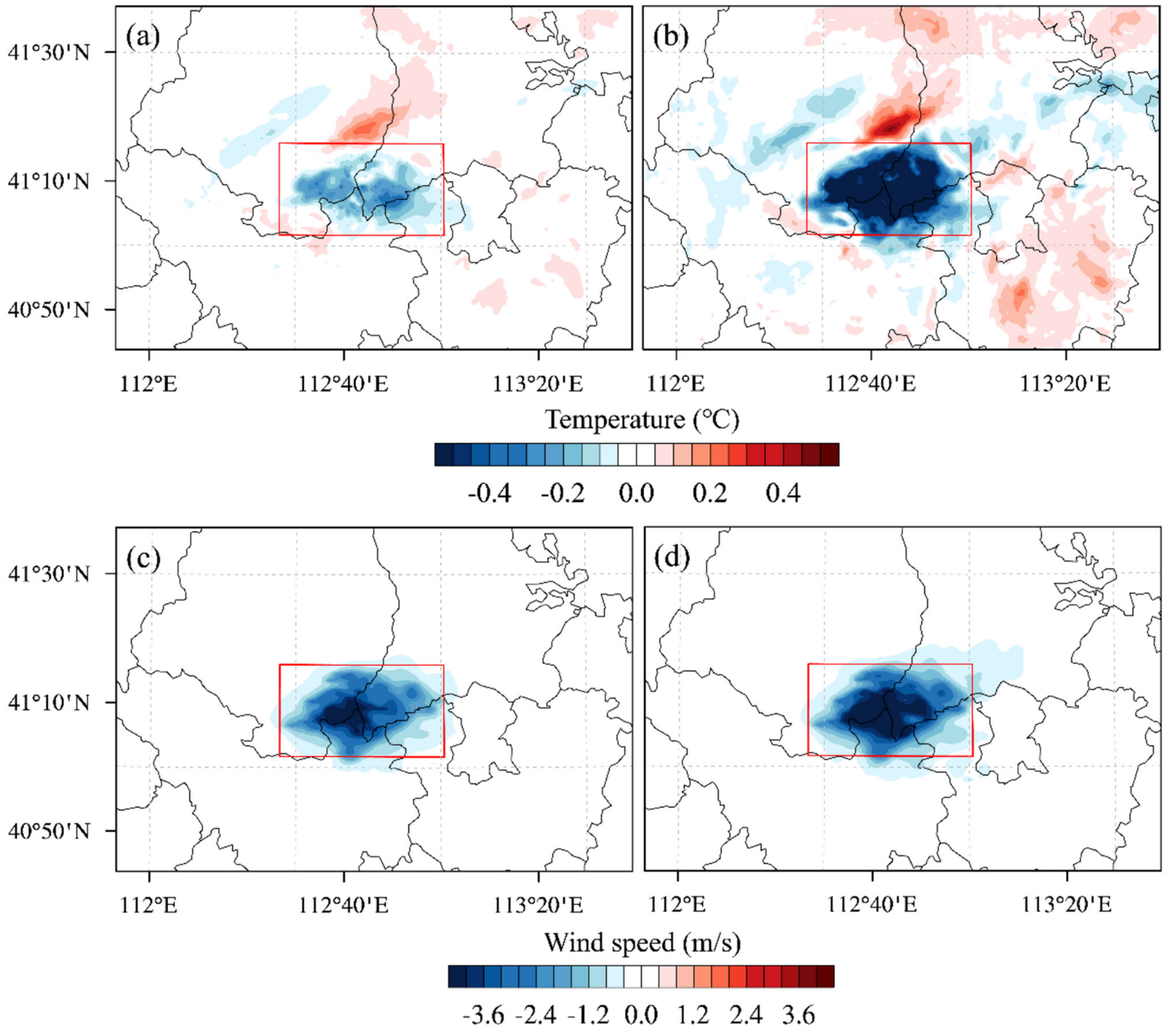

FIGURE 4 | Spatial distribution of mean surface air temperature differences during (a) diurnal and (b) nocturnal periods in winter (units:°C) and spatial distribution of mean wind speed differences at turbine height during (c) diurnal and (d) nocturnal periods in winter (units: m/s). Red boxes indicate turbine locations.

period, with maximum cooling reaching 0.55°C in areas of high turbine density (Figure 4b). In addition, warming zones are identified to the north and southeast of the wind farm. In summer (Figures S1a and S1b), the magnitude of both diurnal and nocturnal surface temperature changes within the wind farm is smaller than in winter.

3.2 | Impact of Wind Farms on Local Surface Relative Humidity

Figure 5 shows the spatial distribution of mean surface relative humidity differences within the wind farm across different seasons. The wind farm affects surface relative humidity both within its boundaries and in adjacent areas. The regional mean relative humidity changes in winter, spring, summer, and autumn are approximately 0.04%, 0.38%, 0.19%, and 0.39%, respectively, while the corresponding natural variability for the four seasons is 5.88%, 5.54%, 4.35%, and 3.50%, indicating that the magnitude of these changes in surface relative humidity remains smaller than the natural variability. Specifically, in winter (Figure 5a), the most complex humidity pattern is observed, characterized by both increases and decreases in mean surface relative humidity within areas of high turbine density. The amplitude of these differences is substantial, reaching approximately ±1.2%. Additionally, surface relative humidity increases in the southern and eastern areas adjacent to the wind farm, while it decreases in the northern adjacent areas. In spring (Figure 5b) and autumn (Figure 5d), the spatial distribution patterns of surface relative humidity differences are similar, with both seasons showing an increase of approximately 1.2% within the wind farm. However, a slight decrease in humidity is observed in the northern part of the wind farm during autumn. The wind farm's influence on mean surface relative humidity is least pronounced in summer (Figure 5c), primarily manifesting as an increase of approximately 0.6% within the wind farm and in western adjacent areas. Conversely, decreases in humidity are observed in the northeastern and southern regions of the wind farm. Except in winter, the spatial distribution pattern of water vapor mixing ratio at 2-m level is largely consistent with that of surface relative humidity, both showing an increasing trend in areas with dense turbines (Figures S2b, S2c, and S2d). In contrast, during winter, the 2 m water vapor mixing ratio decreases by approximately 0.05 g/kg in areas with dense turbines, while changes in surrounding areas are negligible (Figure S2a). This indicates that changes in relative humidity are not solely determined by moisture content but are also influenced by other factors such as temperature.

Figure 6 shows the spatial distribution of mean surface relative humidity differences within the wind farm for diurnal and nocturnal periods. During diurnal periods (Figure 6a), the interior of the wind farm exhibits an increase in humidity, with variations ranging from 0% to 0.6%. In contrast, adjacent northern

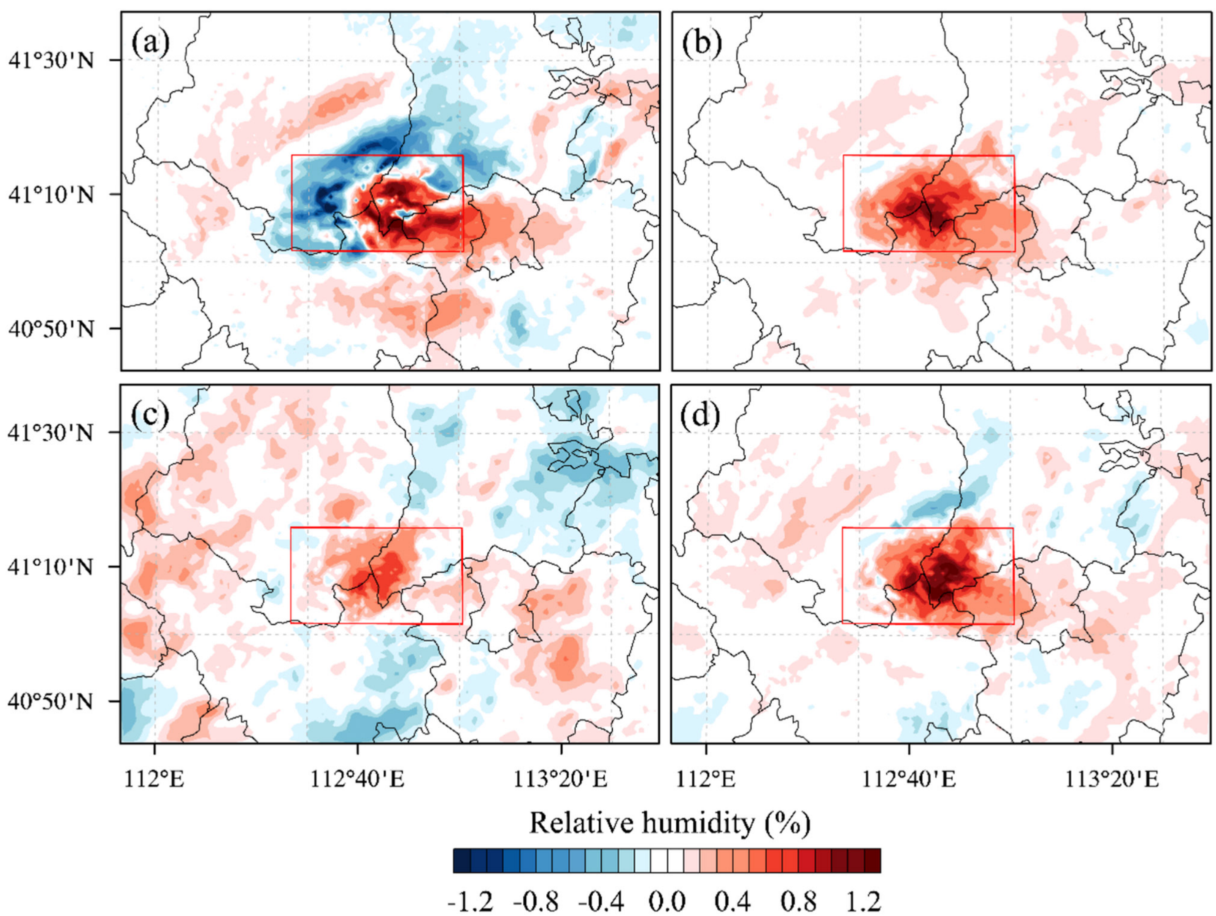

FIGURE 5 | Spatial distribution of mean surface relative humidity differences during (a) winter, (b) spring, (c) summer, and (d) autumn. Red boxes indicate turbine locations. Units: %.

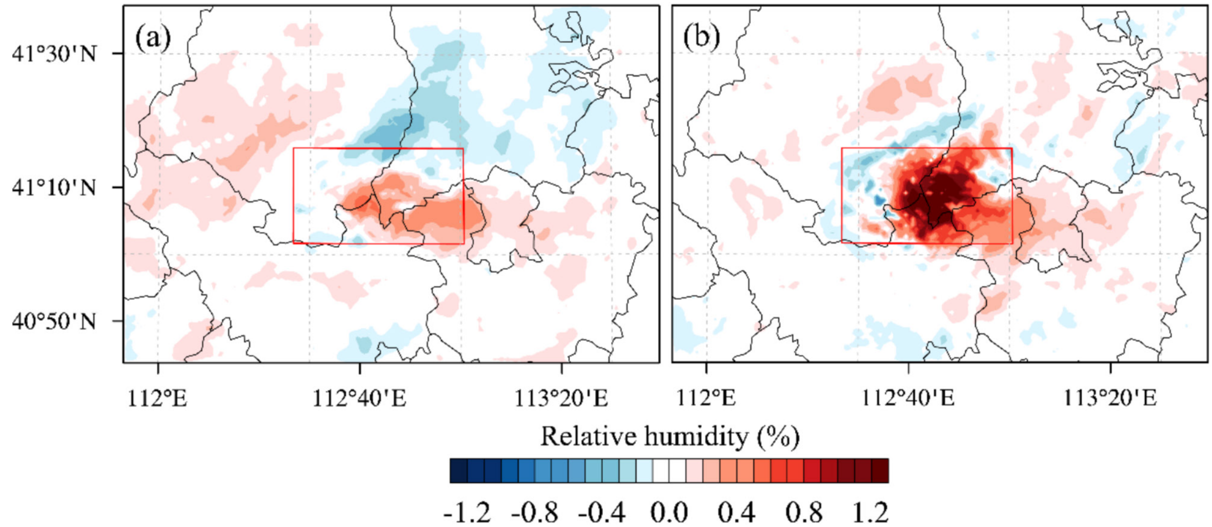

FIGURE 6 | Spatial distribution of mean surface relative humidity differences for (a) diurnal and (b) nocturnal periods. Red boxes indicate turbine locations. Units: %.

areas show a slight decrease in surface relative humidity. The spatial patterns of the 2 m water vapor mixing ratio are broadly consistent with those of surface relative humidity, both showing increases in areas with concentrated turbine distribution and decreases in the northern adjacent areas (Figure S3a). During nocturnal periods (Figure 6b), the humidifying effect of the wind farm is more pronounced, with an intensity approximately twice that during daytime and a broader spatial extent. A marked increase in humidity is evident within the wind farm, with a maximum increase exceeding 1.2%. This humidification effect diminishes gradually from the interior of the wind farm toward the surrounding areas. However, the 2 m water vapor mixing ratio during nocturnal periods exhibits a mixed pattern of increases and decreases both inside the wind farm and in its surrounding areas (Figure S3b).

Figures S4a and S4b illustrate the spatial distribution of mean surface relative humidity differences within the wind farm during diurnal and nocturnal periods in winter. In areas with concentrated turbine distribution, surface relative humidity exhibits a complex pattern characterized by both increases and decreases, with the magnitude of nocturnal humidity changes being approximately twice that of diurnal (Figures S4a and S4b) changes. The spatial distribution of surface relative humidity in summer is more complex. During diurnal periods (Figure S5a), both increases and decreases in relative humidity are observed within the wind farm and its surrounding areas, with variations ranging approximately ±0.6%. During nocturnal periods (Figure S5b), the humidification effect in areas with concentrated turbine distribution is more pronounced than during diurnal periods, with relative humidity increasing by approximately 1.2%, while the surrounding areas exhibit a mixed pattern of humidity increases and decreases.

3.3 | Impact of Wind Farms on Wind Speed at Turbine Height

Figure 7 shows the spatial distribution of mean wind speed differences at turbine height within the wind farm across seasons. The impact of the wind farm on wind speeds at turbine height primarily manifests as a blocking and attenuation effect. The regional mean wind speed reductions in winter, spring, summer, and autumn are approximately 1.93, 1.14, 0.74, and 1.41 m/s, respectively, while the corresponding natural variability for the four seasons is 0.36, 0.48, 0.40, and 0.41 m/s, respectively. The changes in wind speed exceed the range of natural variability in all four seasons. Specifically, the attenuation effect is most pronounced in winter (Figure 7a), with wind speeds decreasing by approximately 4.4 m/s in regions of high turbine density. The pattern exhibits a concentric circular structure, weakening gradually toward the periphery. In spring (Figure 7b) and autumn (Figure 7d), wind speed reductions are within the wind farm, ranging from −0.8 to −3.6 m/s, with negligible differences in surrounding areas. The reduction is weakest in summer (Figure 7c), with internal wind speed reduction of approximately 2.0 m/s. Both the range and magnitude are smaller than in other seasons, possibly attributed to enhanced atmospheric convection and turbulence mixing.

Figure 8 illustrates the spatial distribution of mean wind speed differences at turbine height in the wind farm for diurnal and nocturnal periods. During diurnal periods (Figure 8a), a reduction in wind speed is observed within the wind farm, with a maximum decrease of approximately 2.7 m/s. This reduction occurs primarily in regions with high turbine density, while the surrounding areas show no clear differences. In contrast, during nocturnal periods (Figure 8b), this reduction intensifies considerably, reaching up to 3.3 m/s within the wind farm. Furthermore, the nocturnal reduction not only displays greater magnitude but also extends over a larger area compared to diurnal conditions, while the wind farm's influence on more distant peripheral areas remains negligible.

Figure 4c,d illustrates the spatial distribution of mean wind speed differences at turbine height within the wind farm during diurnal and nocturnal periods in winter. During diurnal periods (Figure 4c), wind speed decreases by approximately 4.0 m/s in areas with dense turbine distribution, while changes in the surrounding areas are negligible. During nocturnal periods

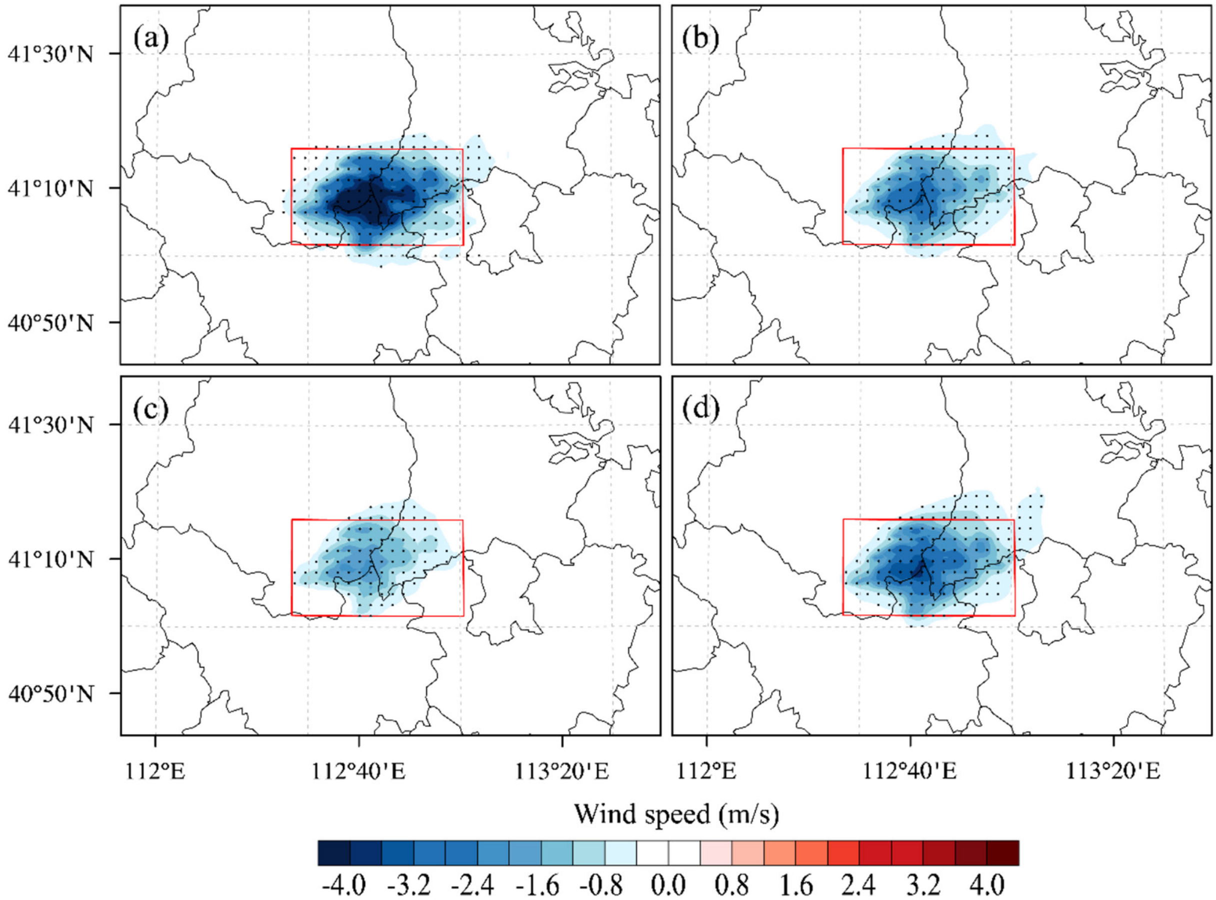

FIGURE 7 | Spatial distribution of mean wind speed differences at turbine height in (a) winter, (b) spring, (c) summer, and (d) autumn. Red boxes indicate turbine locations. Black dots indicate grid cells where mean wind speed differences exceed natural variability. Units: m/s.

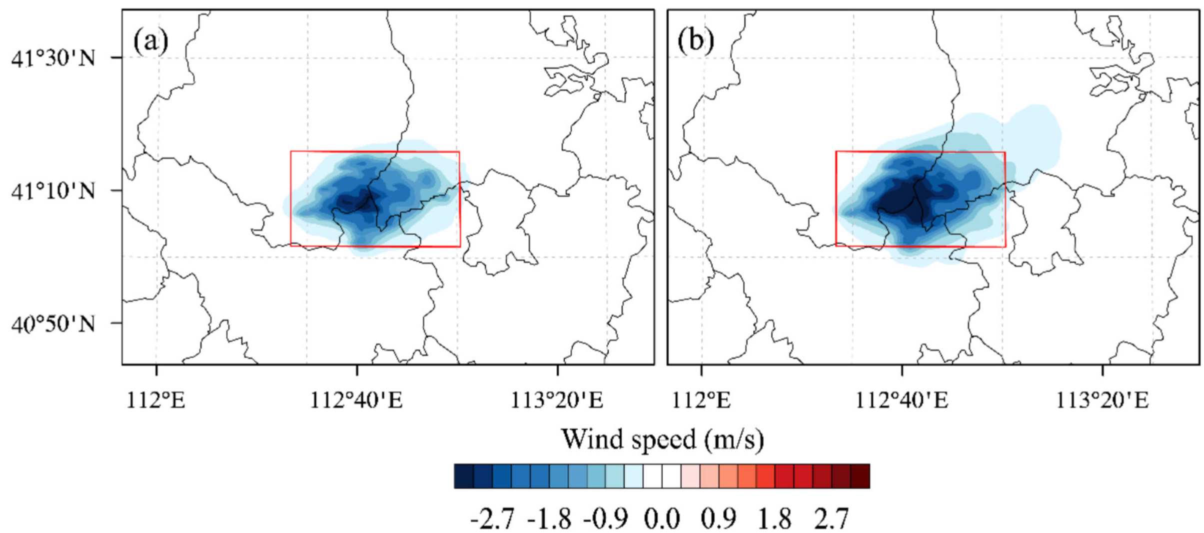

FIGURE 8 | Spatial distribution of mean wind speed differences at turbine height during (a) diurnal and (b) nocturnal periods. Red boxes indicate turbine locations. Units: m/s.

(Figure 4d), the spatial extent of wind speed reduction is greater than during diurnal periods, with wind speed changes diminishing gradually outward in a concentric circular pattern. In summer (Figures S1c and S1d), both diurnal and nocturnal wind speed changes within the wind farm are smaller in magnitude compared to those in winter.

3.4 | Impact of Wind Farms on TKE at Turbine Height

In simulations of wind farm climate effect, turbines serve as both momentum sinks and sources of turbulent kinetic energy. Figure 9 shows the spatial distribution of mean TKE

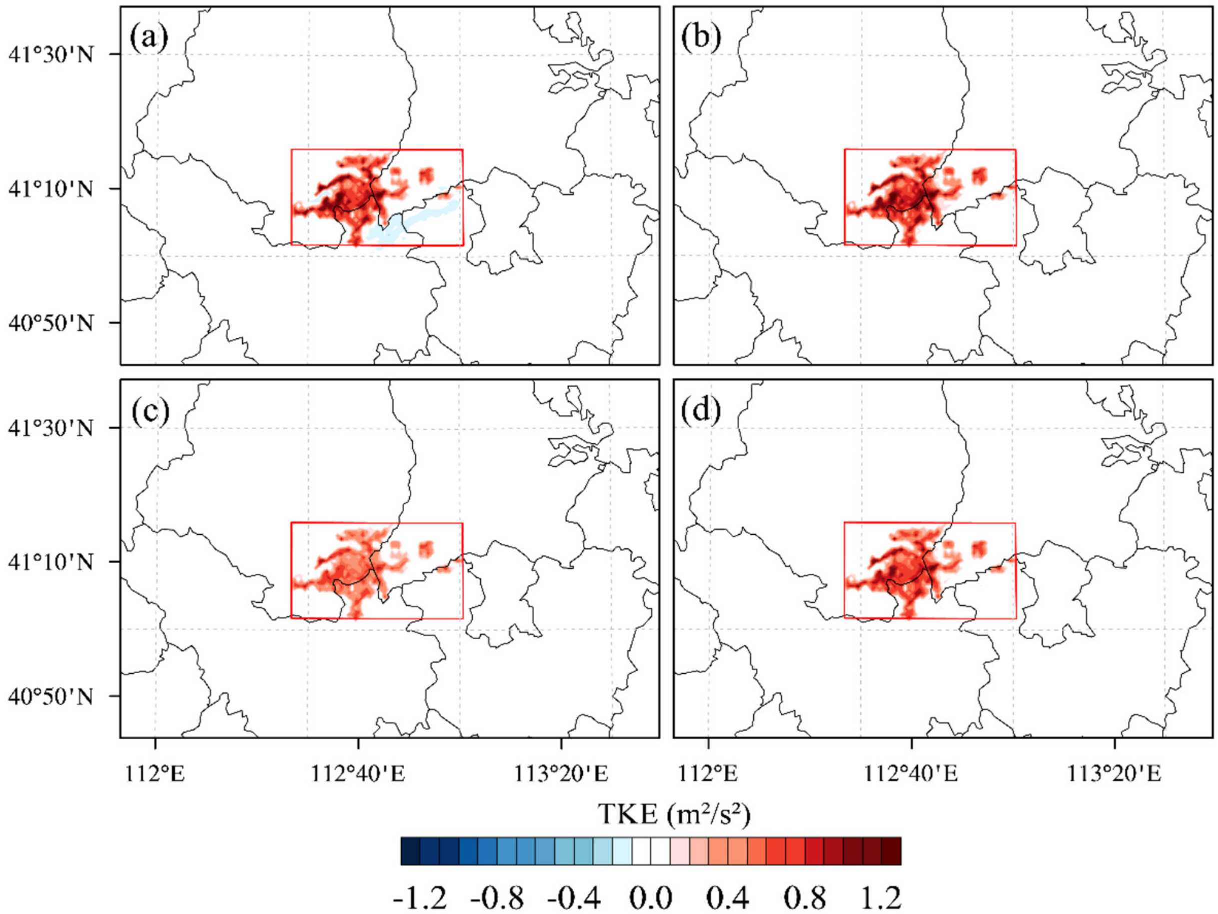

FIGURE 9 | Spatial distribution of mean TKE differences at turbine height during (a) winter, (b) spring, (c) summer, and (d) autumn. Red boxes indicate turbine locations. Units: m^2/s^2.

differences at turbine height within the wind farm across seasons. The wind farm induces noticeable local TKE responses in all seasons, primarily concentrated in areas with high turbine density. In winter (Figure 9a), TKE anomalies exhibit both increases and decreases within the wind farm, although an overall increase prevails, reaching up to $1.2\,m^2/s^2$. Minor TKE decreases are observed at southeastern turbine locations. The spatial patterns of TKE differences in spring (Figure 9b) and autumn (Figure 9d) are similar, with increases within the wind farm and negligible differences in surrounding areas. Notably, the TKE difference in spring is slightly higher than those in autumn. Compared to other seasons, the wind farm has the weakest influence on mean TKE in summer (Figure 9c), producing an increase of approximately $0.7\,m^2/s^2$ within the wind farm and negligible differences in the surrounding areas.

Figure 10 illustrates the spatial distribution of mean TKE differences at turbine height within the wind farm for diurnal and nocturnal periods. During diurnal periods (Figure 10a), TKE enhancement within the wind farm reaches a maximum of $1.2\,m^2/s^2$, while TKE differences in the surrounding areas remain negligible. During nocturnal periods (Figure 10b), the spatial patterns of TKE differences differ slightly from those during diurnal periods. Although overall TKE enhancement is observed within the wind farm, a reduction of approximately $0.2\,m^2/s^2$ occurs in the southeastern part. Notably, the impact of the wind farm on nocturnal TKE is weaker than that during diurnal periods, in contrast to the difference observed for other variables.

Figures S4c and S4d illustrate the spatial distribution of mean TKE differences at turbine height during diurnal and nocturnal periods in winter. During diurnal periods (Figure S4c), TKE increases by up to $1.2\,m^2/s^2$ in areas with dense turbines, while changes in surrounding areas are negligible. During the nocturnal periods (Figure S4d), the magnitude of TKE increase is slightly smaller, with a minor TKE reduction in the southeastern part of the wind farm. In summer (Figures S5c and S5d), both diurnal and nocturnal TKE increases within the wind farm are generally weaker than in winter. Unlike in winter, TKE enhancement prevails throughout the wind farm interior during nocturnal periods in summer.

4 | Discussion

Based on high-resolution WRF simulations of the Huitengxile wind farm, this study reveals the complex impacts of large-scale wind farms on local climate. Wind turbines primarily influence local climate through momentum extraction, turbulence enhancement, and boundary layer mixing. Turbine blades extract momentum from the airflow to generate power, leading to significant wind speed reduction within the wind farm. This effect

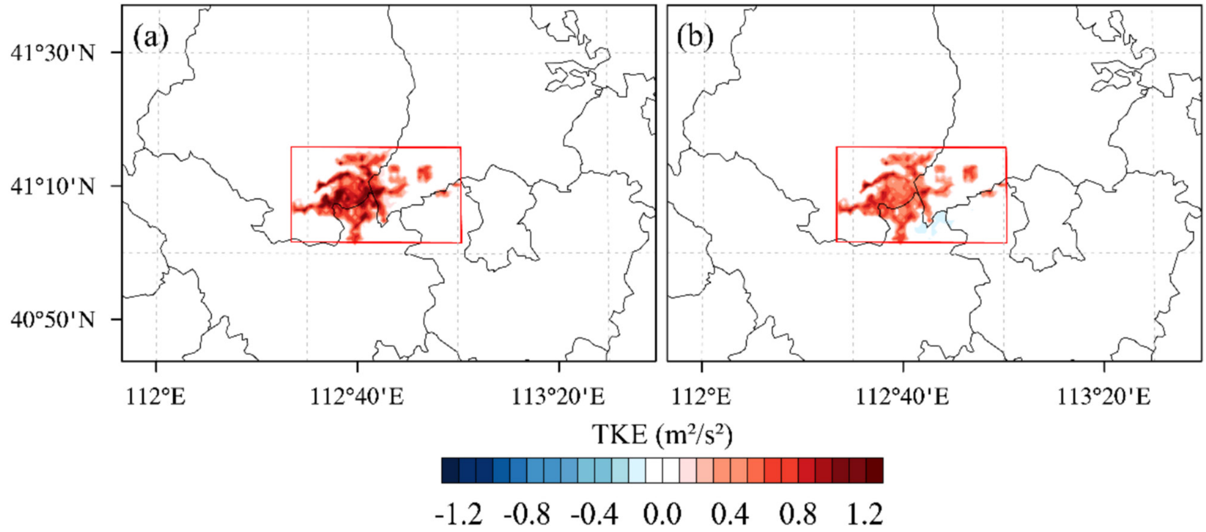

FIGURE 10 | Spatial distribution of mean TKE differences at turbine height during (a) diurnal and (b) nocturnal periods. Red boxes indicate turbine locations. Units: m^2/s^2.

is evident across all seasons and times of day, aligning with previous research [27, 43–45], which further validates the blocking and attenuation effect of large wind farms on wind speed and lends additional credibility to the simulation results of this study. Concurrently, the mechanical disturbance from turbine blades strongly affects the airflow, forming complex wake structures and generating numerous turbulent vortices. Combined with shear instability caused by the altered vertical wind speed distribution, these factors lead to a significant increase in TKE within the wind farm. This is consistent with the findings of Xia et al. [17], indicating that mechanical turbulence induced by turbine blades is the primary source of enhanced TKE in the boundary layer. This further validates the reasonableness of the wind farm parameterization scheme adopted in this study and the reliability of the corresponding simulation results. Furthermore, studies indicate that wind farm impacts are most pronounced near turbine locations, with denser turbine distributions bringing stronger climate responses, indicating that local climate effects of wind farms are closely linked to spatial turbine density.

The results in this study also indicate that the wind farm exhibits distinct seasonal variations in its impact on local climate. The wind farm leads to reduced surface air temperatures, increased surface relative humidity, enhanced TKE at turbine height, and decreased wind speeds at turbine height within the wind farm. These effects are most pronounced in winter and weakest in summer, which can be attributed to the stable stratification and weaker natural turbulent mixing features of the winter atmosphere. Concurrently, background wind speeds are typically higher and more consistent, enabling higher operational efficiency of wind turbines and more intense airflow disturbances. Consequently, the mechanical disturbance effects of wind turbines persist longer within the local environment. In contrast, summer features active atmospheric convection and strong natural turbulence, diluting the disturbance effects of wind farms. Combined with lower and more variable wind speeds, the impact of turbines on airflow is relatively weakened. Regarding variations between diurnal and nocturnal periods, the climatic effects of the wind farm are generally stronger during nocturnal periods than during diurnal periods, manifesting as more pronounced surface cooling and surface humidification effects. However, previous studies have found that wind farm operations cause surface temperatures to exhibit a cooling effect during diurnal periods and a warming effect during nocturnal periods [18, 24]. This discrepancy may relate to wind farm scale. Large-scale wind farms, characterized by numerous densely distributed turbines, significantly disturb the atmospheric boundary layer beyond the influence of medium and small facilities. They persistently alter atmospheric flow patterns over broader areas, with more pronounced turbine interactions and wake superposition effects. This generates more complex local circulation patterns and thermal structures, resulting in distinct response characteristics compared to smaller wind farms. For example, Huang et al. [46], using WRF simulations of large-scale wind farm deployment scenarios over the Three North region of China, found that when the deployment scale reached 3490 GW (approximately 1.75 million turbines), significant summer surface warming exceeding 0.8°C could be induced over North China. This contrasts with the surface cooling effect identified for the Huitengxile wind farm (approximately 1200 turbines) in this study. This discrepancy most likely stems from the substantial difference in wind farm scale between the two studies while also being influenced by differences in spatial resolution, background climate, and terrain conditions, further underscoring that the climatic response of wind farms is strongly dependent on deployment scale, geographic location, and underlying surface characteristics. Notably, the wind speed reduction is stronger during nocturnal periods than during diurnal periods, while the TKE enhancement effect is more pronounced during diurnal periods. This difference primarily stems from the parameterization scheme settings for wind turbines in the WRF simulations. In the WRF simulations conducted for this study, the cut-in and cut-out wind speeds for turbines were set at 3 and 25 m/s, respectively. This means that turbines only operate normally and generate turbulent disturbance effects when wind speeds fall within this range. Because of the differing distribution characteristics of wind speeds between diurnal and nocturnal periods, this parameterization setting resulted in temporal inconsistencies between the wind speed reduction effect and the TKE enhancement effect.

To elucidate the physical processes by which wind farms drive local temperature changes, we examined differences in vertical temperature profiles between scenarios with and without wind farms (Figure 11). The results reveal a characteristic three-layer thermal structure across all seasons and time periods: near-surface cooling, warming at turbine height, and renewed cooling aloft. This universal pattern indicates that wind turbines primarily act as vertical heat redistributors, reorganizing the atmospheric thermal field rather than exerting a uniform warming or cooling effect. In the near-surface layer, large-scale momentum extraction substantially reduces wind speeds below turbine height, weakening the natural wind shear near the surface and thereby diminishing turbulent heat exchange between the surface and the overlying atmosphere. Although the turbines inject considerable TKE, this enhancement is maximized near turbine height and is insufficient to compensate for the reduction in near-surface natural mixing. The resulting vertical decoupling allows nocturnal radiative cooling to accumulate continuously near the surface, producing near-surface cooling. A very shallow cold layer immediately above the ground is evident during diurnal and nocturnal periods in winter and nocturnal periods in summer. This feature is absent during summer diurnal periods, when strong background convection mixing disrupts the near-surface thermal decoupling. Within the rotor-swept layer, intense TKE injection markedly enhances vertical mixing, making the turbine height region a zone of heat convergence. The enhanced turbulent mixing

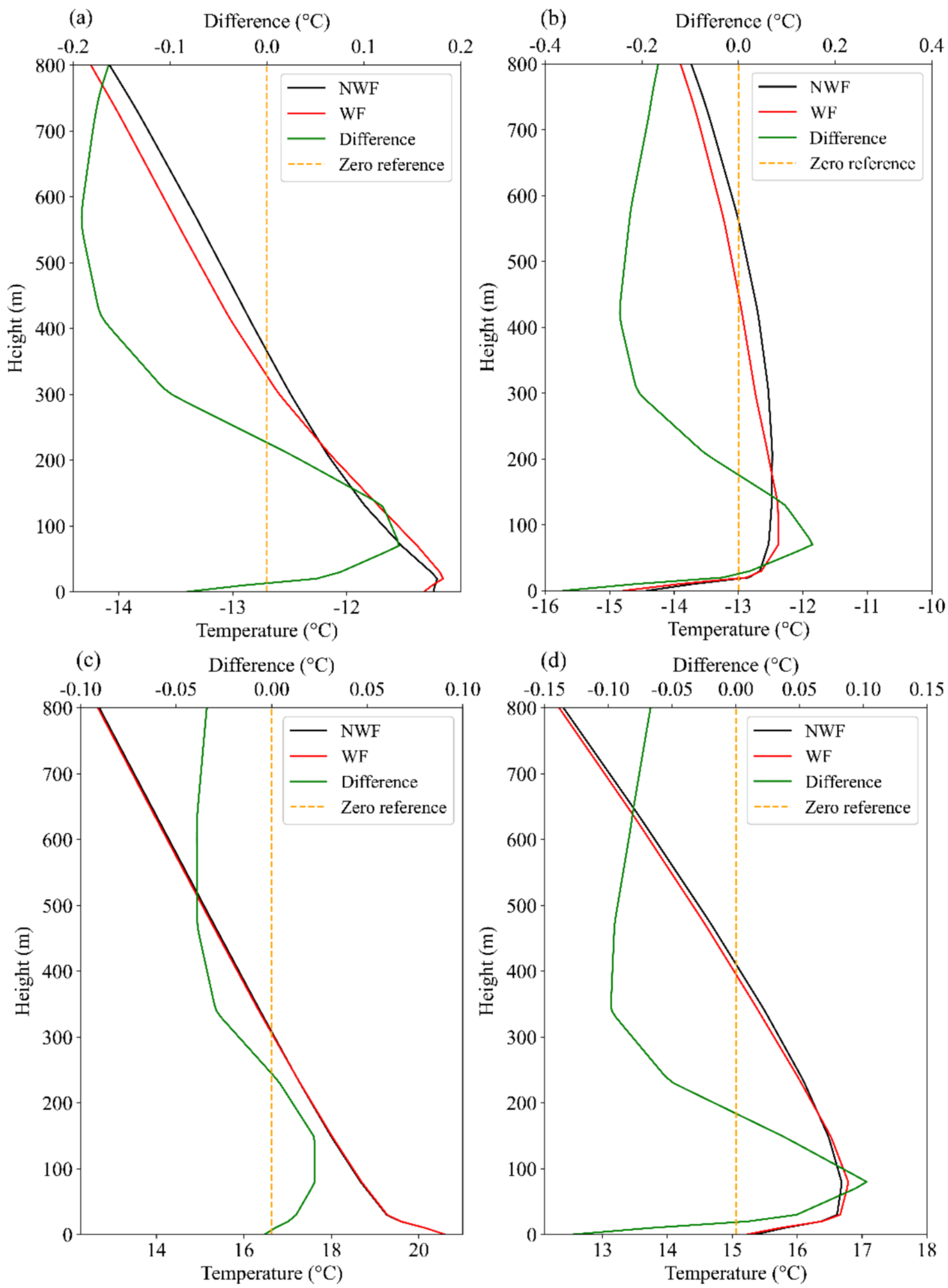

FIGURE 11 | Vertical profiles of air temperature (unit:°C) within the wind farm during (a) winter diurnal, (b) winter nocturnal, (c) summer diurnal, and (d) summer nocturnal periods. NWF and WF denote the simulations without and with the wind farm, respectively.

therefore acts as an efficient "heat pump," transporting sensible heat upward from below and leading to localized warming at turbine height. Above turbine height, the momentum deficit propagates upward while TKE intensity decreases with height, resulting in weakened turbulent mixing and a cooling signal at higher levels. Overall, the physical processes by which wind farms influence local climate can be summarized as a multi-stage driving chain from kinetic energy extraction to thermodynamic response. Wind turbines extract atmospheric momentum through their rotor blades, causing significant wind speed attenuation at turbine height while simultaneously inducing intense mechanical turbulence that substantially elevates TKE within the boundary layer. The enhanced turbulent mixing weakens the stability of atmospheric thermal stratification, drives a systematic rise in planetary boundary layer height, and gives rise to a characteristic three-layer thermal structure in the vertical direction, ultimately resulting in a series of observable changes in near-surface climate variables including air temperature and relative humidity.

Although this study employed high-resolution numerical simulations, it has limitations. First, it used only a single parameterization scheme to simulate the climatic effects of wind farms, failing to adequately consider the sensitivity of simulation results to different parameterizations. Previous research has demonstrated that physical parameterizations such as boundary layer schemes, microphysical processes, and wind farm schemes significantly influence simulation results [47, 48]. Second, this study did not conduct a rigorous statistical significance test on the simulation results. Because of limited computational resources, the simulation period covered only 2018 to 2020, which precluded the analysis of longer term trends and resulted in a sample size of only three for the seasonal mean changes. With such a small sample size, conventional statistical significance tests have limited reliability and applicability and cannot provide robust statistical inference. Future studies could extend the simulation period to conduct long-term simulations, thereby obtaining a sufficient sample size to derive more statistically robust conclusions. Furthermore, this study employs a comparative simulation approach using two scenarios, one with wind farms and one without, to eliminate systematic errors. However, because of the difficulty in obtaining observational data from meteorological masts within the study area, the simulation results could not be validated against in situ measurements, which to some extent limits the reliability of the conclusions. Model validation is critical for ensuring the accuracy of simulation results, and future research will endeavor to acquire observational data through commercial channels or other means to conduct systematic model validation. Despite these limitations, this study contributes to a better understanding of how the large-scale wind farms impact climate and the environment, informing a better balance between wind farm development and environmental protection, providing guidance for the sustainable development of the renewable energy sector.

5 | Conclusions

This study conducted high-resolution numerical simulations of the Huitengxile wind farm in Inner Mongolia using the WRF model, systematically analyzing the impacts of the wind farm on the local climate. The results indicate that the wind farm significantly influenced the local climate. Key effects included reduced surface air temperatures and increased surface relative humidity within the wind farm, along with enhanced TKE at turbine height and weakened wind speeds. These climatic effects were primarily concentrated in areas with high turbine density within the wind farm and had negligible influence on surrounding regions.

The local climate effects of the wind farm exhibit distinct seasonal variations. The most pronounced impact occurs during winter, where surface temperatures decrease by approximately 0.5°C. Spring and autumn show slightly smaller reductions of about −0.4°C, while summer effects are the weakest, with temperature reductions of only 0.2°C. The impact of the wind farm on surface relative humidity is more complex. During winter, both increases and decreases in surface relative humidity coexist within the wind farm. In spring and autumn, the spatial distribution patterns of surface relative humidity differences are similar, with humidity increasing by approximately 1.2%. Summer shows the smallest differences in surface relative humidity, primarily characterized by increased humidity within the wind farm and in western areas, while humidity decreases in the northeastern and southern regions. Additionally, the wind farm leads to a significant increase in TKE within the wind farm. Regarding wind speed response, the weakening effect at turbine height is most pronounced in winter, with wind speeds decreasing by approximately 4.4 m/s. In spring and autumn, wind speed differences at turbine height also exclusively manifest as reductions within the wind farm, ranging from −0.8 to −3.6 m/s. The wind speed weakening effect is relatively weakest in summer, with wind speeds within the wind farm decreasing by approximately 2.0 m/s. The scope and intensity of this effect are also relatively small. Overall, the impact of the wind farm on various meteorological elements is strongest in winter and relatively weak in summer. This seasonal variation may be related to differences in atmospheric stability, wind speed conditions, and the intensity of surface-atmosphere water vapor exchange during different periods.

Regarding variations between diurnal and nocturnal periods, the wind farm generally exerts a stronger influence on local climate during nocturnal periods than that during diurnal periods. During nocturnal periods, surface air temperatures within the wind farm decrease by approximately 0.44°C; surface relative humidity increases significantly, with an impact intensity roughly twice that observed during diurnal periods; the wind speed reduction effect is also more pronounced, affecting a noticeably larger area than during diurnal periods. Notably, the impact of the wind farm on nocturnal TKE is less pronounced than during diurnal periods. Diurnal TKE enhancement reaches 1.2 m^2/s^2, while nocturnal TKE enhancement is approximately 0.8 m^2/s^2. Further analysis of day–night differences in winter and summer reveals that this pattern is evident in both seasons, although the magnitude of responses varies among meteorological variables across seasons. In winter, the nighttime cooling effect of wind farms is approximately three times that of the daytime, with a maximum temperature decrease of 0.55°C in areas of high turbine density. Surface relative humidity exhibits a spatially complex pattern of both increases and decreases during both day and night, with nocturnal variations approximately twice the daytime magnitude. Hub-height wind speed decreases by approximately 4.0 m/s during the day, while the spatial extent of the wind speed reduction expands further at night, attenuating outward in a concentric pattern. Daytime TKE increases by up to 1.2 m^2/s^2, while the nighttime increase is slightly smaller, with a minor reduction appearing in the southeastern portion of the wind farm. The day–night contrast pattern in summer is broadly similar to that in winter, although the magnitude of responses across all variables is generally weaker. This variation between diurnal and nocturnal periods indicates that the wind farm exerts varying degrees of regulatory effects on local temperature, humidity, TKE, and wind fields by disturbing the structure of the atmospheric boundary layer.

This study reveals the local climate effects of large-scale wind farms, providing a crucial scientific basis for rational planning and optimized operation of wind farms. The findings will guide wind farm site selection and layout optimization, assess the ecological and environmental impacts of wind power development, advance the sustainable development of renewable energy, and achieve the harmonious integration of energy development and environmental protection.

Author Contributions

Xiashu Su: conceptualization, methodology, formal analysis, visualization, writing – original draft, writing – review and editing. **Entao Yu:** conceptualization, methodology, software, writing – original draft, writing – review and editing. **Dongwei Liu:** investigation, data curation, funding acquisition, writing – original draft, writing – review and editing.

Acknowledgments

We particularly thank the European Centre for Medium-Range Weather Forecasts for providing the ERA5 reanalysis data. We also extend our sincere gratitude to all the researchers and institutions for providing essential data support for this study.

Funding

This research was funded by the Science and Technology Major Project of Inner Mongolia, "Assessing the Ecological Impacts of Wind and Solar Energy Development in Inner Mongolia and Formulating Adaptive Mitigation Strategies," and the National Key R&D Program of China (2023YFF0803500).

Conflicts of Interest

The authors declare no conflicts of interest.

Data Availability Statement

The datasets generated during this study are available from the authors upon reasonable request.

References

1. Ö. Güler, "Wind Energy Status in Electrical Energy Production of Turkey," *Renewable and Sustainable Energy Reviews* 13 (2009): 473–478.

2. M. Balat, G. Ayar, C. Oguzhan, H. Uluduz, and U. Faiz, "Influence of Fossil Energy Applications on Environmental Pollution," *Energy Sources, Part B: Economics, Planning, and Policy* 2, no. 3 (2007): 213–226.

3. L. Kemp, C. Xu, J. Depledge, et al., "Climate Endgame: Exploring Catastrophic Climate Change Scenarios," *Proceedings of the National Academy of Sciences of the United States of America* 119, no. 34 (2022): e2108146119, https://doi.org/10.1073/pnas.2108146119.

4. Z. Zhang, "Asian Energy and Environmental Policy: Promoting Growth While Preserving the Environment," *Energy Policy* 36 (2008): 3905–3924.

5. M. F. Howland, S. K. Lele, and J. O. Dabiri, "Wind Farm Power Optimization Through Wake Steering," *Proceedings of the National Academy of Sciences of the United States of America* 116, no. 29 (2019): 14495–14500.

6. Y. Qin, Y. Li, R. Xu, et al., "Impacts of 319 Wind Farms on Surface Temperature and Vegetation in the United States," *Environmental Research Letters* 17 (2022): 024026, https://doi.org/10.1088/1748-9326/ac49ba.

7. R. Saidur, N. A. Rahim, M. R. Islam, and K. H. Solangi, "Environmental Impact of Wind Energy," *Renewable and Sustainable Energy Reviews* 15 (2011): 2423–2430.

8. C. Xia and Z. Song, "Wind Energy in China: Current Scenario and Future Perspectives," *Renewable and Sustainable Energy Reviews* 13 (2009): 1966–1974.

9. M. Sawant, S. Thakare, A. P. Rao, A. E. Feijóo-Lorenzo, and N. D. Bokde, "A Review on State-Of-The-Art Reviews in Wind-Turbine- and Wind-Farm-Related Topics," *Energies* 14 (2021): 2041, https://doi.org/10.3390/en14082041.

10. C. M. Smith, R. J. Barthelmie, and S. C. Pryor, "In Situ Observations of the Influence of a Large Onshore Wind Farm on Near-Surface Temperature, Turbulence Intensity and Wind Speed Profiles," *Environmental Research Letters* 8 (2013): 034006, https://doi.org/10.1088/1748-9326/8/3/034006.

11. X. Zhang, J. Li, Z. Chen, et al., "A Preliminary Exploration on the ln Fluence of Wind Farms on Local Climate in Dabie Mountainous Areas in China: A Case Study of Dawu in Hubei Province," *Advances in Meteorological Science and Technology* 9, no. 2 (2019): 56–61. (in Chinese).

12. A. C. Fitch, "Climate Impacts of Large-Scale Wind Farms as Parameterized in a Global Climate Model," *Journal of Climate* 28 (2015): 6160–6180.

13. L. Liu, P. Liu, J. Yu, G. Feng, Q. Zhang, and J. C. Svenning, "Wind Farms Increase Land Surface Temperature and Reduce Vegetation Productivity in the Inner Mongolia," *Geography and Sustainability* 5 (2024): 319–328.

14. L. M. Miller and D. W. Keith, "Climatic Impacts of Wind Power," *Joule* 2 (2018): 2618–2632.

15. S. C. Pryor, R. J. Barthelmie, and T. J. Shepherd, "20% of US Electricity From Wind Will Have Limited Impacts on System Efficiency and Regional Climate," *Scientific Reports* 10 (2020): 541, https://doi.org/10.1038/s41598-019-57371-1.

16. C. Wang and R. G. Prinn, "Potential Climatic Impacts and Reliability of Large-Scale Offshore Wind Farms," *Environmental Research Letters* 6 (2010): 025101, https://doi.org/10.1088/1748-9326/6/2/025101.

17. G. Xia, L. Zhou, J. M. Freedman, S. B. Roy, R. A. Harris, and M. C. Cervarich, "A Case Study of Effects of Atmospheric Boundary Layer Turbulence, Wind Speed, and Stability on Wind Farm Induced Temperature Changes Using Observations From a Field Campaign," *Climate Dynamics* 46 (2016): 2179–2196.

18. S. Baidya Roy and J. J. Traiteur, "Impacts of Wind Farms on Surface Air Temperatures," *Proceedings of the National Academy of Sciences of the United States of America* 107, no. 42 (2010): 17899–17904.

19. R. Chang, R. Zhu, and P. Guo, "A Case Study of Land-Surface-Temperature Impact From Large-Scale Deployment of Wind Farms in

China From Guazhou," *Remote Sensing* 8 (2016): 790, https://doi.org/10.3390/rs8100790.

20. J. M. Walsh-Thomas, G. Cervone, P. Agouris, and G. Manca, "Further Evidence of Impacts of Large-Scale Wind Farms on Land Surface Temperature," *Renewable and Sustainable Energy Reviews* 16 (2012): 6432–6437.

21. L. Zhou, Y. Tian, S. Baidya Roy, C. Thorncroft, L. F. Bosart, and Y. Hu, "Impacts of Wind Farms on Land Surface Temperature," *Nature Clim Change* 2 (2012): 539–543.

22. H. Sun, Y. Luo, Z. Zhao, and R. Chang, "The Impacts of Chinese Wind Farms on Climate," *Journal of Geophysical Research: Atmospheres* 123 (2018): 5177–5187.

23. G. Xia, L. Zhou, J. R. Minder, R. G. Fovell, and P. A. Jimenez, "Simulating Impacts of Real-World Wind Farms on Land Surface Temperature Using the WRF Model: Physical Mechanisms," *Climate Dynamics* 53 (2019): 1723–1739.

24. S. Baidya Roy, "Simulating Impacts of Wind Farms on Local Hydrometeorology," *Journal of Wind Engineering and Industrial Aerodynamics* 99 (2011): 491–498.

25. C. B. Hasager, P. Vincent, J. Badger, et al., "Using Satellite SAR to Characterize the Wind Flow Around Offshore Wind Farms," *Energies* 8 (2015): 5413–5439.

26. R. J. Mangara, Z. Guo, and S. Li, "Performance of the Wind Farm Parameterization Scheme Coupled With the Weather Research and Forecasting Model Under Multiple Resolution Regimes for Simulating an Onshore Wind Farm," *Advances in Atmospheric Sciences* 36 (2019): 119–132.

27. J. K. Lundquist, K. K. DuVivier, D. Kaffine, and J. M. Tomaszewski, "Costs and Consequences of Wind Turbine Wake Effects Arising From Uncoordinated Wind Energy Development," *Nature Energy* 4 (2019): 26–34.

28. A. C. Fitch, J. K. Lundquist, and J. B. Olson, "Mesoscale Influences of Wind Farms Throughout a Diurnal Cycle," *Monthly Weather Review* 141 (2013): 2173–2198.

29. B. H. Fiedler and M. S. Bukovsky, "The Effect of a Giant Wind Farm on Precipitation in a Regional Climate Model," *Environmental Research Letters* 6 (2011): 045101, https://doi.org/10.1088/1748-9326/6/4/045101.

30. R. Vautard, F. Thais, I. Tobin, et al., "Regional Climate Model Simulations Indicate Limited Climatic Impacts by Operational and Planned European Wind Farms," *Nature Communications* 5 (2014): 3196, https://doi.org/10.1038/ncomms4196.

31. T. Zhang, M. Meng, Y. Cao, Y. Jiang, and J. Liu, "Research on Effect of Construction of Huitengxile Wind Farm to Grassland Ecosystem With Transitions of Land Use and Landscape Pattern," *Procedia Engineering* 174 (2017): 780–787.

32. K. S. Lim and S. Hong, "Development of an Effective Double-Moment Cloud Microphysics Scheme With Prognostic Cloud Condensation Nuclei (CCN) for Weather and Climate Models," *Monthly Weather Review* 138 (2010): 1587–1612.

33. M. J. Iacono, J. S. Delamere, E. J. Mlawer, M. W. Shephard, S. A. Clough, and W. D. Collins, "Radiative Forcing by Long-Lived Greenhouse Gases: Calculations With the AER Radiative Transfer Models," *Journal of Geophysical Research – Atmospheres* 113 (2008): D13103, https://doi.org/10.1029/2008JD009944.

34. M. Nakanishi and H. Niino, "An Improved Mellor–Yamada Level-3 Model: Its Numerical Stability and Application to a Regional Prediction of Advection Fog," *Boundary-Layer Meteorology* 119 (2006): 397–407.

35. M. Nakanishi and H. Niino, "Development of an Improved Turbulence Closure Model for the Atmospheric Boundary Layer," *Journal of the Meteorological Society of Japan* 87, no. 5 (2009): 895–912.

36. J. B. Olson, J. S. Kenyon, W. A. Angevine, et al., *A Description of the MYNN-EDMF Scheme and the Coupling to Other Components in WRF–ARW* (Earth System Research Laboratory, Global Systems Division. NOAA Technical Memorandum OAR GSD 61, 2019), https://doi.org/10.25923/n9wm-be49.

37. J. B. Olson, T. Smirnova, J. S. Kenyon, et al., *A Description of the MYNN Surface-Layer Scheme* (National Centers for Environmental Prediction. NOAA Technical Memorandum OAR GSL 67, 2021), https://doi.org/10.25923/f6a8-bc75.

38. H. Hersbach, B. Bell, P. Berrisford, et al., "The ERA5 Global Reanalysis," *Quarterly Journal of the Royal Meteorological Society* 146 (2020): 1999–2049.

39. C. Soci, H. Hersbach, A. Simmons, et al., "The ERA5 Global Reanalysis From 1940 to 2022," *Quarterly Journal of the Royal Meteorological Society* 150, no. 764 (2024): 4014–4048.

40. E. Yu, L. Song, B. Wang, et al., "Investigation on the 2018 Prolonged Freezing Event in South China Using the WRF Model at Convection-Permitting Resolution: Model Performance and Sensitivity Analysis of Physical Parameterizations," *Atmospheric Research* 310 (2024): 107645, https://doi.org/10.1016/j.atmosres.2024.107645.

41. A. C. Fitch, J. B. Olson, J. K. Lundquist, et al., "Local and Mesoscale Impacts of Wind Farms as Parameterized in a Mesoscale NWP Model," *Monthly Weather Review* 140 (2012): 3017–3038.

42. D. Moravec, V. Barták, V. Puš, and J. Wild, "Wind Turbine Impact on Near-Ground Air Temperature," *Renewable Energy* 123 (2018): 627–633.

43. O. García-Santiago, A. Hahmann, J. Badger, A. N. Hahmann, and A. Peña, "Evaluation of Wind Farm Parameterizations in the WRF Model Under Different Atmospheric Stability Conditions With High-Resolution Wake Simulations," *Wind Energy Science* 9 (2024): 963–979, https://doi.org/10.5194/wes-9-963-2024.

44. D. Quint, J. K. Lundquist, N. Bodini, and D. Rosencrans, "Simulated Meteorological Impacts of Offshore Wind Turbines and Sensitivity to the Amount of Added Turbulence Kinetic Energy," *Wind Energy Science* 10 (2025): 1269–1301, https://doi.org/10.5194/wes-10-1269-2025.

45. J. M. Tomaszewski and J. K. Lundquist, "Simulated Wind Farm Wake Sensitivity to Configuration Choices in the Weather Research and Forecasting Model Version 3.8.1," *Geoscientific Model Development* 13 (2020): 2645–2662.

46. J. B. Huang, P. K. Lou, H. W. Sun, Y. Luo, and Z. C. Zhao, "Numerical Experimental Study on the Potential Climatic Impacts of Large-Scale Wind Farms in China," *Advances in Climate Change Research* 10, no. 3 (2019): 143–149, https://doi.org/10.1016/j.accre.2019.10.001.

47. D. Carvalho, A. Rocha, M. Gómez-Gesteira, and C. Silva Santos, "Sensitivity of the WRF Model Wind Simulation and Wind Energy Production Estimates to Planetary Boundary Layer Parameterizations for Onshore and Offshore Areas in the Iberian Peninsula," *Applied Energy* 135 (2014): 234–246.

48. D. E. K. Dzebre and M. S. Adaramola, "A Preliminary Sensitivity Study of Planetary Boundary Layer Parameterization Schemes in the Weather Research and Forecasting Model to Surface Winds in Coastal Ghana," *Renewable Energy* 146 (2020): 66–86.

Supporting Information

Additional supporting information can be found online in the Supporting Information section. **Figure S1:** Spatial distribution of mean surface air temperature differences during (a) diurnal and (b) nocturnal periods in summer (units:°C) and spatial distribution of mean wind speed differences at turbine height during (c) diurnal and (d) nocturnal periods in summer (units: m/s). Red boxes indicate turbine locations. **Figure S2:** Spatial distribution of mean 2 m water vapor mixing ratio differences during (a) winter, (b) spring, (c) summer, and (d) autumn. Red boxes indicate turbine locations. Units: g/kg. **Figure S3:** Spatial distribution of mean 2 m water vapor mixing ratio differences for (a) diurnal and

(b) nocturnal periods. Red boxes indicate turbine locations. Units: g/kg. **Figure S4:** Spatial distribution of mean surface relative humidity differences during (a) diurnal and (b) nocturnal periods in winter (units: %) and spatial distribution of mean TKE differences at turbine height during (c) diurnal and (d) nocturnal periods in winter (units: m^2/s^2). Red boxes indicate turbine locations. **Figure S5:** Spatial distribution of mean surface relative humidity differences during (a) diurnal and (b) nocturnal periods in summer (units: %) and spatial distribution of mean TKE differences at turbine height during (c) diurnal and (d) nocturnal periods in summer (units: m^2/s^2). Red boxes indicate turbine locations.